nature physics
SUPPLEMENTARY INFORMATION
DOI: 10.1038/NPHYS2788

Fourier-transform inelastic X-ray scattering from time- and momentum-dependent phonon–phonon correlations

I. OPTICAL-LASER AND X-RAY CONFIGURATION

The experiment used 70 fs x-ray pulses at 10 keV from the LCLS in the high-charge (250 pC) mode at 120 Hz. The x-ray beam was focused and slitted to a spot with cross section 20 $\times$ 250 μm ^{2} near the sample position. The x-ray fluence was kept below 0.2 mJ/cm^2 to avoid sample damage. The sample was a 1 $\times$ 1 cm^2 (100)-oriented single crystal of Ge oriented at grazing incidence with the normal approximately parallel to the x-ray polarization. The grazing incidence angle was $\alpha = 0.5$ deg. The x-ray bandwidth was $\Delta E/E \sim 10^{-3}$, typical of the natural "pink" beam of the fundamental emmission of the FEL. The sample was held in vacuum to avoid air scattering. The scattering pattern was collected with the Cornell-SLAC Pixel Array Detector (CSPAD)[1] positioned 210 mm behind the sample.

Few mJ, 50 fs infra-red (IR) pulses centered at 800 nm were derived from a Ti:sapphire multi-pass amplifier and were focused to a spot with a transverse cross section 60 $\times$ 400 μm^2 at the sample position. Typical incident fluences were $<$ 20 mJ/cm^2 at 2 deg incidence. The laser was polarized in the plane of incidence. Laser-off images were collected by dropping every 24th laser pulse. The fine timing between laser and x-ray pulses was established by the initial decrease in the 111 diffraction peak in a laser-excited Bi film[2].

II. DATA ANALYSIS

Each laser-on image is an average of 50 $-$ 300 single exposures. Laser-off images were averages of $\sim$ 2500 exposures. The time-resolved images were first subtracted to obtain $\Delta I(t)$ and then binned down to 515 $\times$ 512 pixels (supplemental movie1). This improves the pixel noise and it makes the data more manageable without significant loss in momentum resolution. The images were sorted based on the arrival time of the electron bunch measured by the phase cavities at the end of the undulator hall, which improves the timing resolution down to $\sim$ 250 fs[3].

The CSPAD area detector consists of 32 individual rectangular tiles. In order to correct for the strong background fluctuations of each tile, a series of tungsten wires in front of the detector served as a zero-photon calibration. The shadow cast by the wires were used to

DOI: 10.1038/NPHYS2788

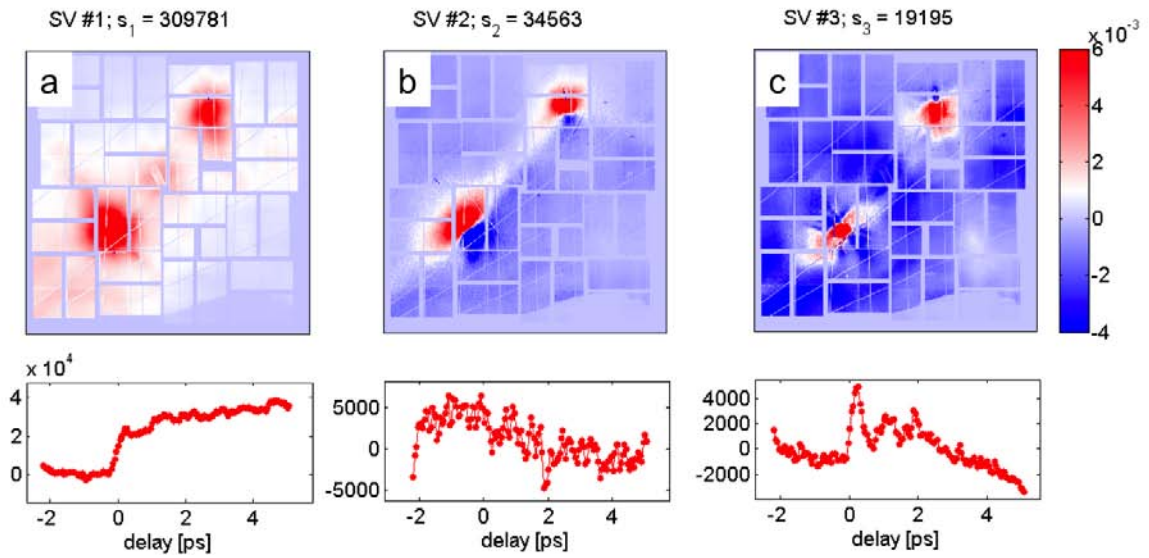

FIG. 1. The first three singular vectors in the SVD of the time resolved data. The top panel shows the U matrix and the lower panel shows the corresponding rows of sV^t.

correct for the fluctuating offsets of each tile independently and a flat-field image from Cu fluorescence was used to correct for gain variations across the detector before binning.

A. Data filtering by singular value decomposition

The procedure for removing the slowly varying background is based on singular value decomposition (SVD). This method has been successfully applied to the analysis of time-resolved data[4, 5]. Although subtracting a moving average yields similar results, we found that truncating the SVD as shown below is more effective at removing the FEL wavelength fluctuations.

Each frame in the time-resolved data is arranged as a column vector x_j of size $N_p \cdot N_p \times 1$, where $N_p \cdot N_p$ is the number of pixels. These vectors are stacked into the columns of matrix X of size $N_p \cdot N_p \times N_t$, with N_t the number of time points. The decomposition of matrix X in its singular vectors yields $X = USV^T$, where U and V are orthogonal matrices and S is a diagonal matrix with the singular values s_j arranged in descending order in its diagonal. The columns of matrix U denoted by u_j represent time-independent image patterns (when rearranged to size $N_p \times N_p$) that contain the partial q-dependence of the scattering, while the columns of V are of size $N_t \times 1$ and contain only time dependent information[4, 5].

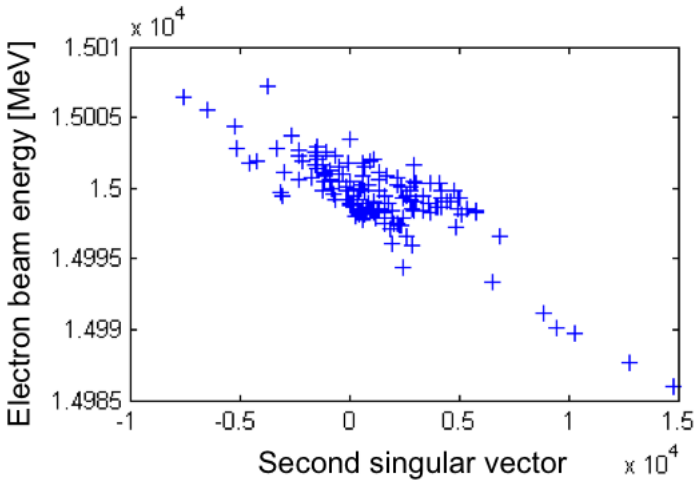

FIG. 2. Correlation between the second right singular vector in Fig. 1 and the electron beam energy which gives a measure of the x-ray wavelength.

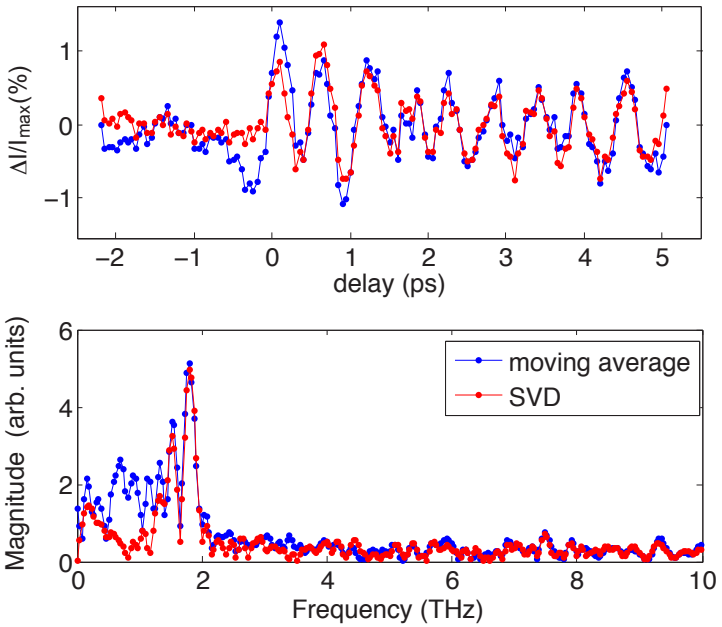

FIG. 3. Comparison of the two methods to remove the slowly varying background: SVD and a moving average. The top panel shows the filtered time-dependence and the bottom panel its Fourier transform.

Figure 1 shows the first three singular vectors (SVs) in the SVD decomposition of the time-domain data. The top row represents the column vectors u_j (rearranged to 512×512) and the bottom row is the corresponding column of the product $S \cdot V^t$. The first SV represents

DOI: 10.1038/NPHYS2788

the average signal and can be removed by subtracting the average of each pixel, however the intensity shift observed in the second SV [blue and red areas in Fig. 1 (b) top panel] is a clear signature of the x-ray wavelength drift. There is a clear correlation between the right singular vector, V, of the second component (Fig. 1 (b) bottom panel), with the measured electron energy loss (which is a measure of the x-ray wavelength), as shown in Fig. 2. This shows that a large part of the variance in the data is due to x-ray wavelength fluctuations (which result in the scattering pattern shifting). These fluctuations are uncorrelated with the pump-probe response of the sample, and since the SVD is a diagonalization of the covariance matrix, it separates these uncorrelated variables into different singular vectors[6].

Figure 3 (top panel) shows the time-dependence of a representative pixel and its Fourier transform (bottom panel) after reconstructing the signal (the matrix X) ignoring the first two SVs shown above. This procedure is compared with the result of subtracting a moving average to the time-dependent data. Clearly the signal is not degraded while the SVD can remove most of the FEL fluctuations, especially at $t < 0$. The filtered data (supplemental movie2), and those shown in Figs. 2 and 3 of the main text are obtained by reconstructing the matrix X ignoring the first two singular vectors.

III. THEORY

The thermal diffuse scattering intensity at momentum transfer $\mathbf{Q}$ due to one-phonon scattering is [7, 8]

$$I(\mathbf{Q}) \propto \sum_j \frac{1}{\Omega_j(\mathbf{q})} \left(n_j(\mathbf{q}) + \frac{1}{2} \right) |F_j(\mathbf{Q})|^2 , \tag{1}$$

where Ω_j is the phonon frequency and $n_j = [\exp(-\hbar\Omega_j/k_BT) - 1]^{-1}$ is the Bose-Einstein phonon population for branch j at temperature T. The inelastic structure factor $F_j(\mathbf{Q})$ is given by a sum over all atoms in the unit cell[7–9]

$$F_j(\mathbf{Q}) = \sum_s \frac{f_s}{\sqrt{m_s}} e^{-W_s} (\mathbf{Q} \cdot \mathbf{e}_{s,j,\mathbf{q}}) e^{-i\mathbf{K}_Q \cdot \mathbf{r}_s}, \tag{2}$$

here f_s, m_s, W_s and $\mathbf{r}_s$ are the atomic scattering factor, the mass, the Debye-Waller factor and the position of atom s in the unit cell, $\mathbf{K}_Q$ is the closest reciprocal lattice vector to $\mathbf{Q}$.

The phonon polarization, $\mathbf{e}_{s,j,\mathbf{q}}$, and frequency, $\Omega_j(\mathbf{q})$, in Eq. (1) and (2) were obtained

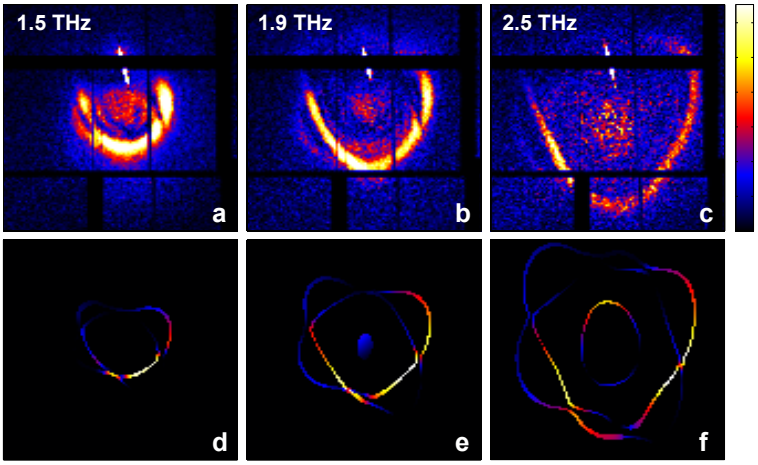

FIG. 4. (a) - (c) Fourier-transform data shown in the upper panel on Fig. 3 of the main text. (d) - (f) calculations of the inelastic structure factor $|F_j(\mathbf{Q})|^2$ using a Born model of the forces.

from the dynamical matrix constructed using a Born-von-Karman model with harmonic forces up to six nearest neighbors[10, 11].

A. Inelastic structure factor contribution

Figures 4 and 5 show the measured intensity distribution at various frequencies (top rows show the same data as Fig. 3 of the main text), compared with $|F_j(\mathbf{Q})|^2$ as defined by Eq. (2) (bottom rows). The contours in the lower panels of Figs. 4 and 5 show the calculated $|F_j(\mathbf{Q})|^2$ for positions of q-space and branch j where the phonon dispersion intersects the ω plane indicated.

[1] P. Hart, S. Boutet, G. Carini, M. Dubrovin, B. Duda, D. Fritz, G. Haller, R. Herbst, S. Hermann, C. Kenney, N. Kurita, H. Lemke, M. Messerschmidt, M. Nordby, J. Pines, D. Schafer, M. Swift, M. Weaver, G. Williams, D. Zhu, N. Van Bakel, and J. Morse, SPIE Proceedings **8504**, 85040C (2012).

[2] D. M. Fritz, D. A. Reis, B. Adams, R. A. Akre, J. Arthur, C. Blome, P. H. Bucksbaum, A. L. Cavalieri, S. Engemann, S. Fahy, R. W. Falcone, P. H. Fuoss, K. J. Gaffney, M. J. George, J. Hajdu, M. P. Hertlein, P. B. Hillyard, M. Horn-von Hoegen, M. Kammler, J. Kaspar,

DOI: 10.1038/NPHYS2788

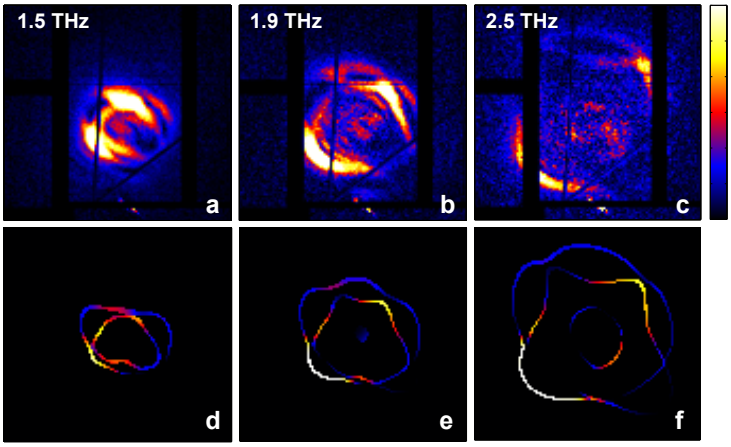

FIG. 5. (top row) Fourier-transform data shown in the lower panel on Fig. 3 of the main text. (bottom row) calculations of the inelastic structure factor $|F_j(\mathbf{Q})|^2$ using the Born model of the forces discussed in the text.

R. Kienberger, P. Krejcik, S. H. Lee, A. M. Lindenberg, B. McFarland, D. Meyer, T. Montagne, . D. Murray, A. J. Nelson, M. Nicoul, R. Pahl, J. Rudati, H. Schlarb, D. P. Siddons, K. Sokolowski-Tinten, T. Tschentscher, D. von der Linde, and J. B. Hastings, Science **315**, 633 (2007), http://www.sciencemag.org/content/315/5812/633.full.pdf.

[3] J. M. Glownia, J. Cryan, J. Andreasson, A. Belkacem, N. Berrah, C. I. Blaga, C. Bostedt, J. Bozek, L. F. DiMauro, L. Fang, J. Frisch, O. Gessner, M. Gühr, J. Hajdu, M. P. Hertlein, M. Hoener, G. Huang, O. Kornilov, J. P. Marangos, A. M. March, B. K. McFarland, H. Merdji, V. S. Petrovic, C. Raman, D. Ray, D. A. Reis, M. Trigo, J. L. White, W. White, R. Wilcox, L. Young, R. N. Coffee, and P. H. Bucksbaum, Opt. Express **18**, 17620 (2010).

[4] E. Henry and J. Hofrichter, in *Numerical Computer Methods*, Methods in Enzymology, Vol. 210, edited by M. L. J. Ludwig Brand (Academic Press, 1992) pp. 129 – 192.

[5] Eric R. Henry, Biophysics Journal **72**, 652 (1997).

[6] I. T. Jolliffe, *Principal Component Analysis*, 2nd ed. (Springer, 2002).

[7] Ruqing Xu and Tai C. Chiang, Z. Kristallogr. **220**, 1009 (2005).

[8] B. E. Warren, *X-Ray Diffraction* (Dover, New York, 1969).

[9] M. Trigo, J. Chen, V. H. Vishwanath, Y. M. Sheu, T. Graber, R. Henning, and D. A. Reis, Phys. Rev. B **82**, 235205 (2010).

[10] Helen M. J. Smith, Phil. Trans. Roy. Soc. Lond. **241**, 105 (1948).

[11] Frank Herman, J. Phys. Chem. Solids **8**, 405 (1959).